Journal Pre-proof

Equilibrium distribution of diethyl phthalate plasticiser in cellulose acetate-based materials: Modelling and parameter estimation of temperature and composition effects

Simoní Da Ros, Argyro Gili, Katherine Curran

PII: S0048-9697(22)04799-4

DOI: https://doi.org/10.1016/j.scitotenv.2022.157700

Reference: STOTEN 157700

To appear in: *Science of the Total Environment*

Received date: 13 April 2022

Revised date: 27 June 2022

Accepted date: 25 July 2022

Please cite this article as: S. Da Ros, A. Gili and K. Curran, Equilibrium distribution of diethyl phthalate plasticiser in cellulose acetate-based materials: Modelling and parameter estimation of temperature and composition effects, *Science of the Total Environment* (2022), https://doi.org/10.1016/j.scitotenv.2022.157700

Equilibrium distribution of diethyl phthalate plasticiser in cellulose acetate-based materials: modelling and parameter estimation of temperature and composition effects

Simoní Da Ros[†*], Argyro Gili[†], Katherine Curran[†*]

[†] UCL Institute for Sustainable Heritage, University College London, 14 Upper Woburn Place, London WC1H 0NN, United Kingdom.

[*]Correspondence authors: s.ros@ucl.ac.uk (Simoní Da Ros), k.curran@ucl.ac.uk (Katherine Curran).

Abstract: Understanding the transport and fate of semi-volatile organic compounds (SVOCs) such as phthalates in indoor environments is fundamental for quantifying levels of human exposure and preventing adverse health effects. In this context, the partition coefficient of phthalates between indoor built materials and/or consumer goods and the surrounding atmosphere represents a key parameter for determining concentration distributions. Partition coefficients are also of fundamental importance for describing degradation phenomena associated with plasticiser loss from polymeric materials. However, this key parameter has only been determined for a limited number of systems and environmental conditions. Here, we assess the partitioning behaviour of the diethyl phthalate (DEP) plasticiser in cellulose acetate (CA)-based materials for the first time, determining the effects of temperature and plasticiser composition on equilibrium distributions at temperatures between 20 and 80 ˚C and using CA samples with DEP contents ranging from 6 to 22wt%. Additionally, we propose a model to describe and quantify the effect of temperature and plasticiser composition, with model parameters being estimated using non-linear regression and measurements from 130 distinct experiments. Finally, we assess the suitability of our developed model to simulate the migration of DEP from CA-based materials.

Keywords: phthalates; DEP; cellulose acetate; plasticiser loss; partition coefficients.

1. Introduction

The assessment of indoor air quality plays a crucial role in determining levels of human exposure to pollutant compounds which can cause adverse health effects. Semi-volatile organic compounds (SVOCs) such as phthalates are of particular concern, as they have been associated with increased risks of endocrine disruption, cancer, birth defects, and type 2 diabetes (Miles-Richardson, 2017; Mondal and Mukherjee, 2020). These compounds are added to consumer goods or building materials and can migrate to their surrounding environment over time, being therefore found in significant levels indoors (Fromme et al., 2004; Sheu et al., 2021; Yang et al., 2020).

To determine emission levels from indoor materials, the knowledge of the material/air partition coefficient, *K*, is of fundamental importance, as it defines the equilibrium distribution of the compound of interest between the two phases (Huang and Jolliet, 2016; Xu and Little, 2006). However, this key parameter has only been determined for a limited number of systems and environmental conditions (Huang and Jolliet, 2019; Liu et al., 2014). For phthalates, di-2-ethylhexyl phthalate (DEHP), benzyl butyl phthalate (BBP), di-n-butyl phthalate (DnBP) and di-isobutyl phthalate (DiBP) exemplify some of the compounds receiving the most attention, with studies reporting the partitioning of these compounds between polyvinyl chloride (PVC) floorings and air (Cao et al., 2016; Liang and Xu, 2014), among other sink materials (Wei et al., 2018).

Meanwhile, other phthalates have been investigated to a lesser extent, including diethyl phthalate (DEP), which represents one of the first plasticisers employed in the industrial production of semi-synthetic plastics in the late 19th and early 20th century, and that is still used in the manufacture of several consumer goods (Da Ros and Curran, 2021;

Koniecki et al., 2011). The partition coefficient of DEP is also a key parameter for describing degradation phenomena associated with plasticiser loss in modern and contemporary artworks and historic artefacts based on polymeric materials. Of particular interest in this work is the partition coefficient of DEP between air and the semi-synthetic polymer cellulose acetate (CA), which finds applications in several consumer goods including textiles, plastics, films, cigarette filters and food packaging, among others (Puls et al., 2011; Rajeswari et al., 2020).

CA is also found in heritage collections as part of modern art and design objects, in 20th century social history objects and in film and photographic archival materials. It is known as one of the least stable plastics in museums, presenting significant conservation challenges. A key degradation pathway associated with CA-based materials involves the loss of plasticisers, which can lead to embrittlement. Plasticiser loss can also make CA more hydrophilic (del Gaudio et al., 2021), accelerating the rate of hydrolytic degradation reactions which can lead to the complete collapse of its integrity (Sutherland et al., 2012). However, without the knowledge of the partitioning behaviour of common CA plasticisers, such as DEP, it is not possible to describe mathematically the migration extent of these compounds from CA-based materials to the environment, or to quantitatively relate this physical process to additional chemical degradation pathways associated with CA-based goods. To the best of our knowledge, no studies have yet investigated the partition coefficient of DEP in CA-based materials. This paper aims to address this gap.

In our previous study (Da Ros and Curran, 2021), we quantified the equilibrium distribution of DEP on glass and aluminum surfaces, given the importance of these materials in indoor environments, scientific laboratory tools and instruments and in the storage and display cases involving historic CA-based objects. Herein, we feed this knowledge in the investigation of DEP equilibrium distributions in CA-based materials – for the first time,

determining the effect of temperature and CA plasticiser composition on the partition coefficient of DEP between CA and its surrounding environment, $K_{CA\text{-}air}$. To achieve this, we performed equilibration experiments at seven temperatures ranging from 20 to 80 ˚C, using CA samples containing three different DEP compositions which ranged from 6 to 22 wt%, totalling 21 investigated experimental conditions. Additionally, we propose a model to describe and quantify the effect of temperature and DEP content on $K_{CA\text{-}air}$. Finally, we assess the suitability of our proposed $K_{CA\text{-}air}$ model for describing the migration of DEP from CA-based materials.

2. Materials and Methods

2.1 Synthesis of diethyl phthalate plasticised cellulose acetate

DEP plasticised CA samples containing either 6, 14 or 22wt% DEP were prepared as described elsewhere (Da Ros et al., 2021a), using the solvent casting method. This composition range was selected in order to obtain miscible blends and avoid phase separation (Bao et al., 2015). In a typical procedure, plasticised CA containing 22wt% of DEP was prepared by dissolving DEP (6.8 g) (99.5%, Sigma-Aldrich, Product code 524972) in acetone (25 mL) (99 %, Alfa Aesar, used as received), before the addition of CA (24 g) (Sigma-Aldrich, Product Code 180955), followed by the addition of further acetone (50 mL) (Da Ros et al., 2021a). The resultant mixture was kept under reflux for 4.5 h with continuous stirring, allowed to cool for 1 h with stirring and finally poured over a flat glass tray. Slow solvent evaporation was allowed for 1 week by keeping a glass lid over the sample tray at room temperature. The final drying procedure was performed in a vacuum oven (150 mbar) for 96 h at 20 ˚C. Fig S1 in the Supplementary Information (*SI*) further illustrates the preparation steps and Table S1 summarises the amounts of DEP, CA and acetone used in the synthesis of plasticised CA samples containing 6, 14 or 22 wt% DEP. Samples were cut to form square-

shaped pieces (0.5 cm x 1 cm x 1 mm) and stored at 5 °C prior to equilibration experiments. Throughout this work, these samples are labelled as *x-DEP/CA*, where *x* represents the plasticiser content in wt%. DEP contents in wt% of produced *x-DEP/CA* samples were quantified by infrared spectroscopy, as described in Section 2.3, being equal to 5.4 ± 0.33, 12.46 ± 0.57 and 25.12 ± 0.65 for *6-DEP/CA*, *14-DEP/CA* and *22-DEP/CA* samples, respectively.

2.2 Equilibration experiments

Sample enclosures used in this work consisted of 20, 120 and 250 mL borosilicate glass vials equipped with a lid presenting an aluminum inner surface, which were purchased either from Fisher Scientific (London, catalogue number 12383317 for 20 mL vials) or Ampulla (London, for 120 and 250 mL vials), Fig. S2 and Table S2 in the Supplementary Information (*SI*). Vials were dried at 150 ˚C (glass) and 90 ˚C (lid) for 12 h prior to experiments to minimise contamination. Sample enclosures of different volumes were used to enable significant plasticiser loss to occur at different experimental conditions.

To measure the equilibrium concentration ratios of DEP between cellulose acetate and its surrounding gas-phase, DEP plasticised CA samples were individually placed at the centre of enclosure vials, as illustrated by Fig. 1(a-b).

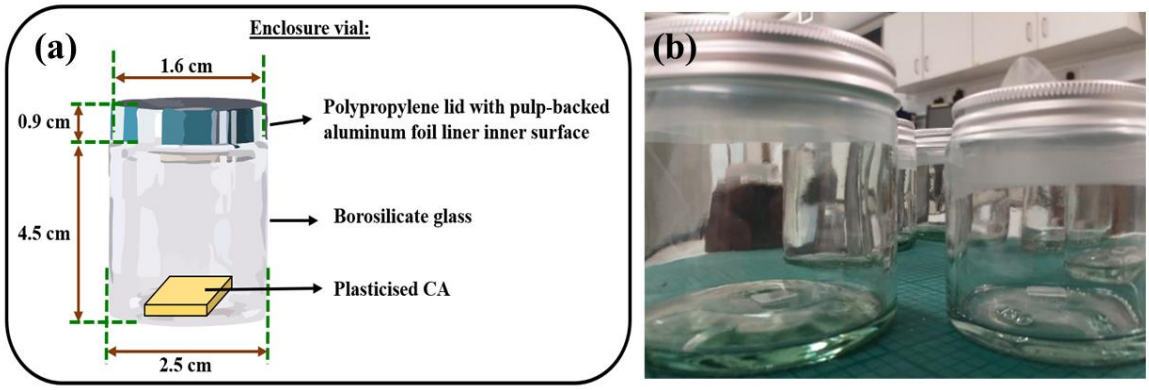

Fig. 1 – Illustrations of *x-DEP/CA* samples within the 20 mL (a), and 120 and 250 mL (b) sample enclosure vials.

Immediately before this step, each sample was analysed for its dimension, weight, and DEP content, as detailed in the next section. After the enclosure vial was sealed, the system was then equilibrated at different temperatures (20, 30, 40, 50, 60, 70 or 80 ˚C) for different periods of time which varied between 20 and 125 days, by keeping the vials in Carbolite ovens (for conditions between 30 and 80 ˚C) and in a room with artificial air conditioning control (for the condition at 20 ˚C). This range of temperature has been chosen to keep the plasticised CA samples below their glass transition temperature (Bao et al., 2015). The actual temperature and relative humidity (RH) during the experimental period were monitored using TinyTag dataloggers. It should be noted that the relative humidity inside enclosure vials was allowed to naturally vary with the temperature, resulting in relatively dry environments (RH smaller than 20% for temperatures higher than 30˚C, Table 1) and therefore minimising the influence of concurrent hydrolytic degradation processes at the investigated conditions. Additionally, the RH fluctuation within the room with artificial air conditioning control (at 20 ˚C) meant that the resulting RH of approximately 50% represented common environmental conditions in museums and galleries worldwide (Bickersteth, 2014).

Samples with each of the three DEP concentrations (6, 14 or 22 wt%) were evaluated at each temperature, resulting in 21 distinct experimental conditions. In addition, at least 3 equilibration times were used at each condition to assess for equilibration, and each experimental condition of temperature, initial DEP content and equilibration time was performed in triplicate to guarantee reproducibility, totalling 178 experiments.

2.3 Quantification of DEP in CA samples

At the end of each stabilisation time, sample vials were removed from ovens and allowed to stabilise at room temperature for approximately 1 h. This was performed to minimise fluctuations that would otherwise be present were samples analysed while still hot. Samples were then removed from vials and immediately had their masses measured gravimetrically. Sample dimensions were also measured at this step, using a digital caliper. Following mass and dimension measurements, samples were immediately analysed to quantify their DEP content by ATR-FTIR.

ATR-FTIR measurements were recorded in a Bruker Platinum-ATR-FTIR equipped with a diamond cell, as described elsewhere (Da Ros et al., 2021a). Spectra were baseline corrected by fixing the average absorbance obtained between 2000 and 2200 cm^{-1} at zero before the extraction of individual band intensities. For each sample, four different locations at each sample surface were analysed. The ratio between the maximum absorbance intensity observed around 748 cm^{-1} and 602 cm^{-1} was used for quantification (Gautam et al., 2016; Richardson et al., 2014) and the peak ratio was calibrated using independent CA reference materials containing known amounts of DEP (0, 6, 10, 14, 20 and 22 wt%), Fig. S3 and Eq. (S1). It is important to note that despite the surface nature of the ATR-FTIR technique, our previous work (Da Ros et al., 2021b) has demonstrated how plasticiser concentration gradients throughout CA cross-sections can be expected to reduce and disappear over time, as the sample equilibrates with its surrounding environment, supporting our methodology for quantifying both bulk and surface DEP concentrations using ATR-FTIR. Thus, bulk concentrations were calculated by averaging measurements from both sample surfaces.

All infrared spectra were batch-processed multiple times using a routine written in Fortran90, which performed the baseline correction, extracted absorbance intensities, calculated the DEP content using the calibration equation and averaged resultant contents for

each sample spectra group. The algorithm workflow is illustrated in Fig. S4. This procedure was applied to enable faster processing of acquired spectra and minimise chances for human error from manual manipulation of individual spectra, since thousands of spectra had to be processed. A copy of the routine is available upon request from the authors.

2.4 Defining the DEP partitioning behaviour between CA and air

The partition coefficient of DEP between CA and air, $K_{CA\text{-}air}$, was defined as the ratio between the equilibrium surface concentration of DEP in CA, in mg·m^{-3}, $C_{DEP,CA}$, and the equilibrium concentration of DEP on the surrounding gas-phase, in mg· m^{-3}, $C_{DEP,gas}$, Eq. (1).

$$K_{CA-air} = \frac{C_{DEP,CA}}{C_{DEP,gas}} \quad (1)$$

While $C_{DEP,CA}$ was calculated from the dimensions, mass and ATR-FTIR measurements, $C_{DEP,gas}$ was inferred from the difference between the amount of DEP lost by the CA sample and the amount adsorbed on the vial inner surfaces during the experiment period, Eq. (2). In Eq. (2), $m_{DEP,CA,0}$ and $m_{DEP,CA,eq}$ represent the mass of DEP in the whole CA sample before and after the equilibration period, respectively, m_{glass} and m_{Al} represent the amount of DEP adsorbed on the glass and aluminum surfaces, respectively, and V_{gas} denotes the free gas-phase volume within the sample enclosure vial.

$$C_{DEP,gas} = \frac{(m_{DEP,CA,0} - m_{DEP,CA,eq}) - m_{glass} - m_{Al}}{V_{gas}} \quad (2)$$

The amounts of DEP adsorbed on the inner vial surfaces, m_{glass} and m_{Al}, were calculated using Eq. (3) and (4), where A_{glass} and A_{Al} represent the glass and aluminum inner surface areas of the sample enclosure vial (detailed in Table S1), and $K_{glass\text{-}air}$ and $K_{Al\text{-}air}$ are the glass and aluminum partition coefficients of DEP at the experiment temperature (in *m*), calculated using Eq. (S2-S3), as detailed in our previous work (Da Ros and Curran, 2021).

$$m_{glass} = K_{glass-air} \cdot A_{glass} \cdot C_{DEP,gas} \quad (3)$$

$$m_{Al} = K_{Al-air} \cdot A_{Al} \cdot C_{DEP,gas} \quad (4)$$

Thus, $C_{DEP,gas}$ can be described by Eq. (5), which results from substituting Eqs. (3) and (4) into Eq. (2).

$$C_{DEP,gas} = \frac{(m_{DEP,CA,0} - m_{DEP,CA,eq})}{\left(V_{gas} + K_{glass-air} \cdot A_{glass} + K_{Al-air} \cdot A_{Al}\right)} \quad (5)$$

2.5 Modelling the effect of temperature and initial DEP content on $K_{CA\text{-}air}$

The dependence of $K_{CA\text{-}air}$ on the temperature and the initial DEP content was described using Eq. (6), a reparameterised version of the van't Hoff equation (Da Ros and Curran, 2021), where T is the temperature, in K, T_{ref} is a reparameterisation constant, defined as equal to 323.15, wt_0 is the initial mass fraction of DEP, in wt%, and k_1, k_2, k_3, k_4, k_5 and k_6 are the parameters estimated from experimental data using non-linear regression, as detailed in the next section. Finally, Eq. (9) defines the relationship between the B constant and the DEP polymer-air phase change enthalpy, ΔH°, where R is the ideal gas constant.

$$K_{CA-air} = \exp\left(A + B\left(\frac{T - T_{ref}}{T}\right)\right) \quad (6)$$

$$A = k_1 + k_2 \cdot wt_0 + k_3 \cdot wt_0^{\,2} \quad (7)$$

$$B = k_4 + k_5 \cdot wt_0 + k_6 \cdot wt_0^{\,2} \quad (8)$$

$$B = \frac{\Delta H^{\circ}}{R \cdot T_{ref}} \quad (9)$$

2.6 Parameter estimation and statistical methods

The estimation of the six parameters from Eq. (6) was performed through the minimisation of the weighed-least-squares objective function (Da Ros et al., 2017; Schwaab and Pinto, 2007), $F_{obj}(\theta)$, Eq. (10), in which *NE* is the number of experimental data points, $K_{CA\text{-}air,j}^{exp}$ denotes the experimental value of the partition coefficient at the experimental condition *j* as calculated from Eq. (1-5), $K_{CA\text{-}air,j}^{mod}$ is the value predicted using Eq. (6), x_j^{exp} represents the experimental condition of temperature and initial DEP content, θ represents a vector with the best set of parameter estimates, and σ_j^2 denotes the variance associated with measurement fluctuations of $K_{CA\text{-}air,j}^{exp}$ at the experiment condition *j*.

$$F_{obj}(\theta) = \sum_{j=1}^{NE} \frac{\left(K_{CA-air,j}^{\exp} - K_{CA-air,j}^{\mathrm{mod}}(x_j^{\exp}, \theta)\right)^2}{\sigma_j^2} \tag{10}$$

The minimisation of Eq. (10) was performed using a hybrid optimisation method implemented in Fortran 90, in which the Particle Swarm Optimization (PSO) algorithm (Kennedy, J., Eberhart, 1995) is used in the initial phase of minimisation (Noronha et al., 1993; Schwaab et al., 2008). The best estimate of the minimum point is used as an initial guess for a second estimation round, using the Gauss-Newton method (Da Ros et al., 2017; Schwaab and Pinto, 2007). The initial phase of minimisation using the PSO algorithm was performed using 30 particles and 10000 iterations, resulting in 100000 evaluations of the objective function. Convergence was achieved when the relative modification of the objective function was smaller than $1 \cdot 10^{-6}$. The statistical significance of the parameter estimates was assessed with the standard t-test (Box, G.P., Hunter, J.S., Hunter, 2005), with a 95 % confidence level. Finally, the evaluation of the model adequacy was performed by comparing the final value of the objective function ($F_{obj}(\theta)$) with the limits of the *Chi-square* distribution with *NE-6* degrees of freedom and 95 % confidence level (Schwaab and Pinto, 2007). In addition, model predictions were compared with experimental measurements, in which prediction errors were calculated by Eq. (11). In this equation, ***B*** is the sensitivity matrix that

contains the first derivatives of the model responses in respect to the model parameters and $\boldsymbol{V_y}$ denotes the covariance matrix of experimental fluctuations (Schwaab et al., 2008).

$$\widehat{\boldsymbol{V}}_y = \boldsymbol{B}\left[\boldsymbol{B}^T\boldsymbol{V}_y\boldsymbol{B}\right]^{-1}\boldsymbol{B}^T \tag{11}$$

2.7 Simulating the DEP loss

The concentration of DEP within the CA pieces was simulated assuming one-dimensional transient diffusion, according to Eq. (12), where $D_{DEP\text{-}CA}$ represents the DEP diffusion coefficient within the polymer matrix, t denotes time and x represents the spatial dimension along which the DEP is diffusing (Little et al., 1994; Xu and Little, 2006).

$$\frac{\partial C_{DEP,CA}}{\partial t} = D_{DEP-CA}\frac{\partial^2 C_{DEP,CA}}{\partial x^2} \tag{12}$$

The initial condition assumed uniform DEP distribution throughout the CA sample dimension. It was assumed that no DEP loss occurred from the bottom surface of the CA piece, which was resting on the glass surface of the vial, Eq. (13) (see Fig. S3).

$$\left.\frac{\partial C_{DEP,CA}}{\partial x}\right|_{x=0} = 0 \tag{13}$$

The second boundary condition was defined through the DEP mass balance on the gas-phase, Eq. (14), where the four terms represent the accumulation of DEP in the air, the interaction and sorption of DEP on the glass and aluminium inner surfaces of the sample enclosure, and the mass flux diffusing out of the CA surface of area A_s, respectively, with $C_{DEP,gas} = 0$ as the initial condition.

$$V_{gas}\frac{\partial C_{DEP,gas}}{\partial t} = -A_{glass}\cdot K_{glass}\frac{\partial C_{DEP,gas}}{\partial t} - A_{Al}\cdot K_{Al}\frac{\partial C_{DEP,gas}}{\partial t} + A_s\cdot D_{DEP-CA}\left.\frac{\partial C_{DEP,CA}}{\partial x}\right|_{x=surface} \tag{14}$$

Additionally, equilibrium was assumed to exist between the DEP concentration at the CA surface and the gas-phase, Eq. (15), where $K_{CA\text{-}air}$ is described according to Eq. (6).

$$C_{DEP,CA} = K_{CA-air} C_{DEP,gas} \tag{15}$$

Finally, the plasticiser loss was simulated using Eq. (16), where $C_{DEP,CA,0}$ is the initial concentration of DEP and $C_{DEP,CA,t}$ is the simulated concentration at time *t*, obtained from solving Eq. (12).

$$DEP\ loss = \frac{\left(C_{DEP,CA,0} - C_{DEP,CA,t}\right) \times 100}{C_{DEP,CA,0}} \tag{16}$$

Values for V_{gas}, A_{glass} and A_{Al} varied according to the sample enclosure vial dimensions (Table S1). For $D_{DEP\text{-}CA}$, an arbitrarily high diffusion coefficient was selected to allow for the simulation of equilibrium concentrations at short equilibration times, as illustrated in Fig. S5 of the *SI*, where $D_{DEP\text{-}CA}$ was taken as equal to $1.5 \cdot 10^{-13}$ $m^2 \cdot s^{-1}$ from our previous work (Gili et al., 2019). Additionally, due to the significantly higher DEP diffusion coefficient in the gas-phase, $D_{DEP,gas}$, when compared to its value within the polymer matrix, we assumed that the DEP mass balance in the gas phase can be approximately described by Eq. (14).

A numerical solution was achieved by discretising Eq. (12) in the space domain using the finite difference method with a central three-point approximation, using 60 discretisation points (Pinto and Lage, 2001). The resultant system of 61 ordinary differential equations was then solved numerically using the backward differentiation technique available in DASSL code in Fortran 90 (Petzold, 1982), with relative and absolute tolerances equal to 10^{-6}. Further details about the numerical solution as implemented in Fortran90 are presented in the *SI*.

3. Results

3.1 Assessment of equilibrium

Fig. 2 (a-f) presents experimentally measured values of plasticiser loss as a function of time for *6-DEP/CA* samples equilibrated in 20 mL vials at different temperatures between 20 and 70 ˚C (values obtained for samples with other DEP concentrations and at other conditions are presented as Fig. S6-S8 in the *SI).* Approximately constant values for plasticiser loss can be observed, within observed experimental uncertainties, with no indication of significant increasing trends, suggesting therefore that systems had reached equilibrium. Additionally, as expected, DEP loss increased with temperature, Fig. 1(a-f), and was lower (in terms of percentage DEP loss) for samples with higher initial plasticiser contents when experiments were performed using vials of the same volume, as illustrated in Fig. S9 in the *SI*. Thus, we used different vial volumes to enable the quantification of plasticiser loss in significant amounts at different experimental conditions, and, therefore, the measurement of $K_{CA\text{-}air}$.

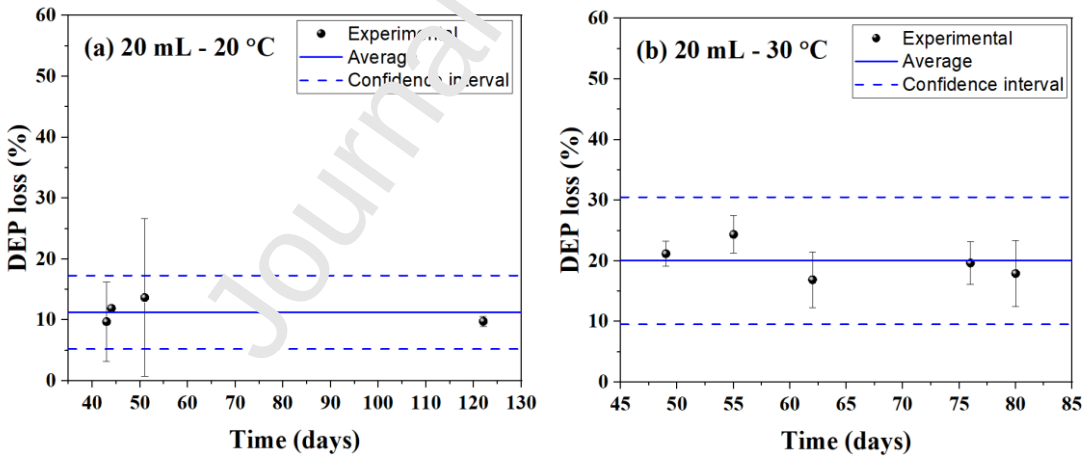

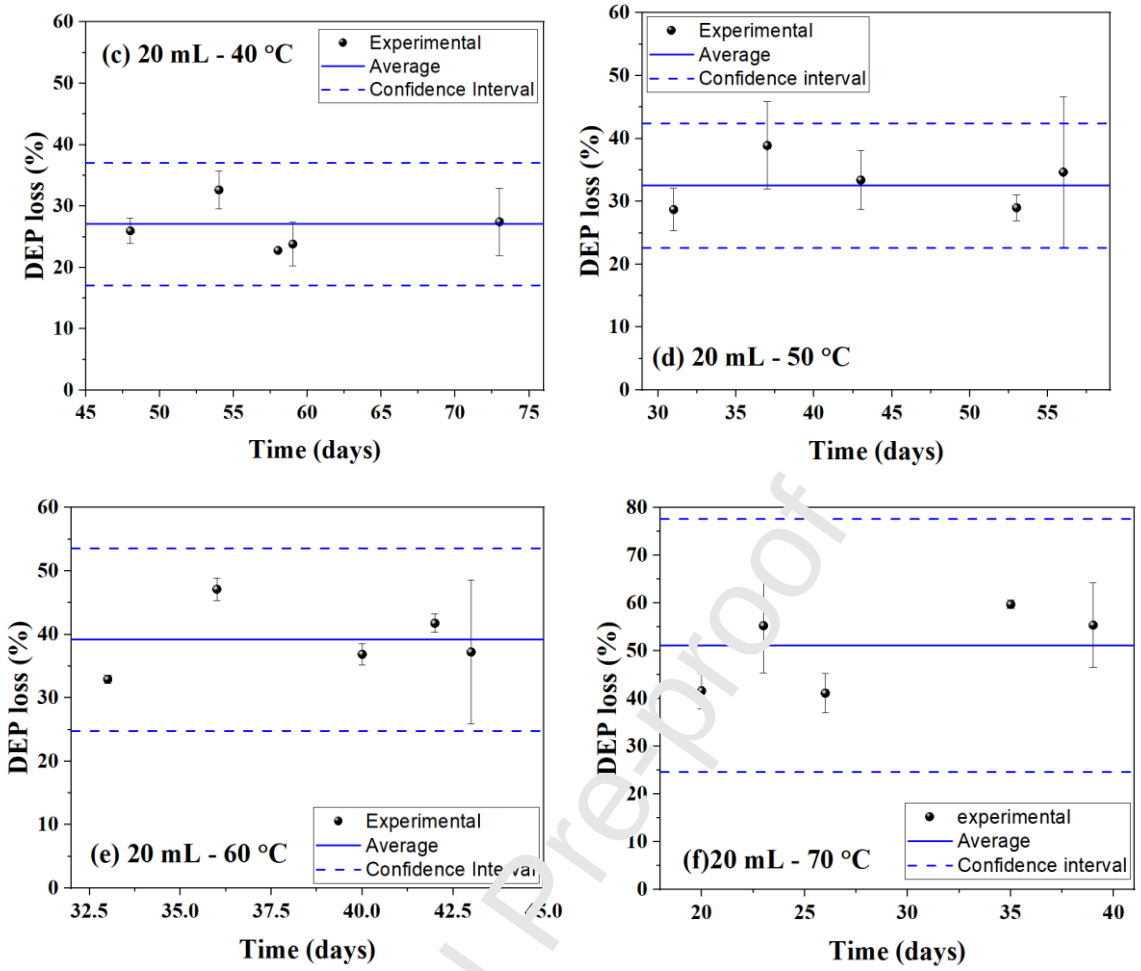

Fig. 2 - Experimental DEP mass loss as a function of time at 20 (a), 30 (b), 40 (c), 50 (d), 60 (e), and 70 (f) ˚C for *6-DEP/CA* samples equilibrated in 20 mL vials. Values obtained at 80 ˚C are illustrated in Fig. S7 in the *SI*.

3.2 Modelling the effect of temperature and initial DEP content on $K_{CA\text{-}air}$

Fig. 3 (a-c) presents experimental $K_{CA\text{-}air}$ averages as a function of temperature for the three ranges of initial DEP contents investigated, while Table 1 summarises averages obtained at each experimental condition, along with their associated standard deviations. As it can be seen, $K_{CA\text{-}air}$ was exponentially reduced as a function of temperature, as expected due to the increased release of volatile DEP from the plastic at higher temperatures, while $K_{CA\text{-}air}$ increased with DEP content, ranging between approximately $4.1 \cdot 10^6 \pm 8.9 \cdot 10^4$ and $1.3 \cdot 10^7 \pm 2.9 \cdot 10^6$ among investigated samples at 20 ˚C.

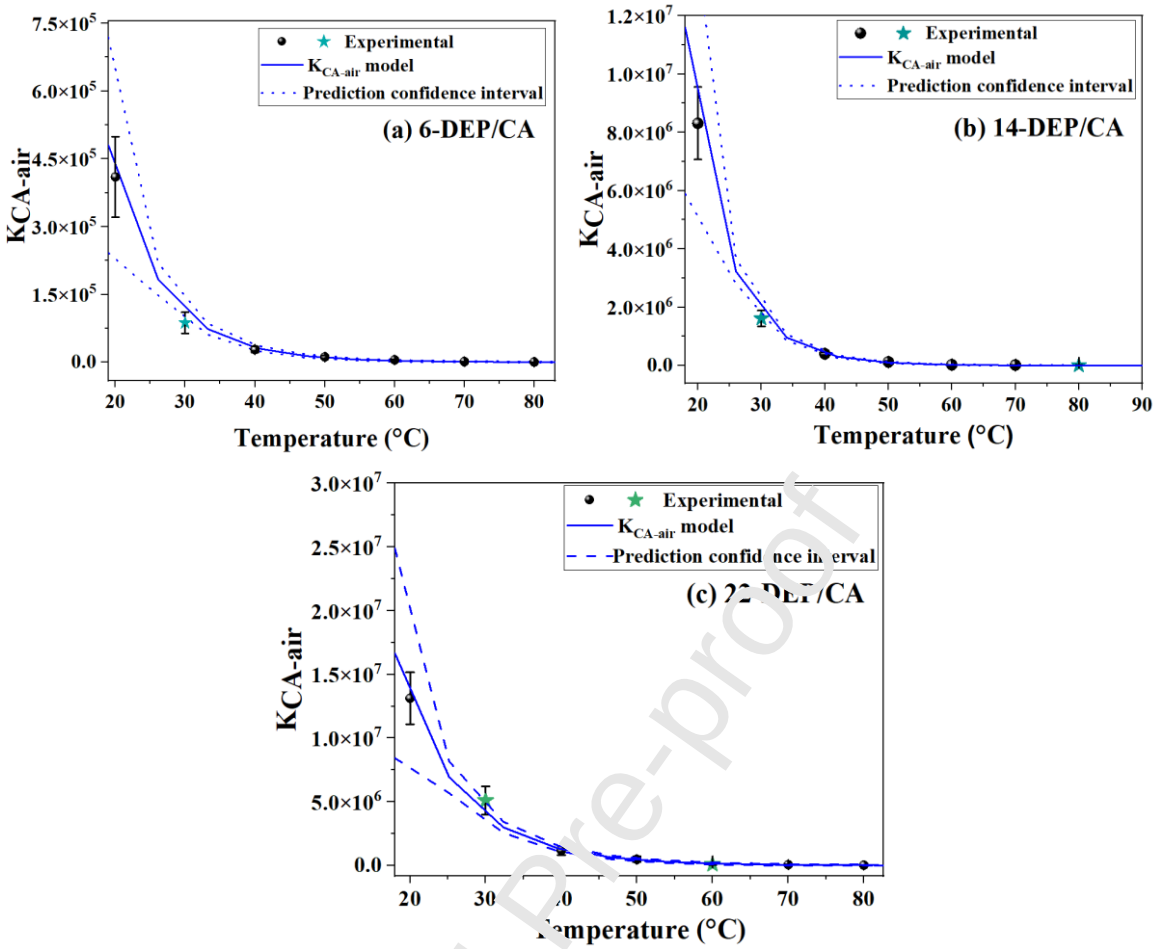

Fig. 3 - Experimental (●,★) and predicted (—) $K_{CA\text{-}air}$ values as a function of equilibration temperature for 6 (a), 14 (b) and 22-DEP/CA (c) samples. The symbol '●' denotes data sets used in the parameter estimation and '★' indicates measurements used as an independent validation set. The linear correlation coefficient between observed and predicted $K_{CA\text{-}air}$ was equal to 0.99.

Table 1 – Experimental conditions of temperature, relative humidity, initial DEP content and resultant $K_{CA\text{-}air}$ averages used as input in the parameter estimation procedure of Eq. (6).

Temperature (˚C)	**Relative Humidity (%) [a]**	**Initial DEP content (wt%) [a]**	**Experimental $K_{CA\text{-}air}$** (unitless)	
			Average	**Standard deviation**
20	51 ± 6.4	25.12 ± 0.65	1.31×10^{7}	2.03×10^{6}
30	**17 ± 2.1**		**5.11×10^{6} [b]**	**1.11×10^{6} [b]**
40	16.4 ± 2.4		1.19×10^{6}	3.61×10^{5}
50	8.6 ± 1.7		4.88×10^{5}	2.19×10^{5}

60	**6.1 ± 0.7**		**9.47×10^4**	**3.12×10^4**
70	5.9 ± 0.5		6.46×10^4	2.14×10^4
80	4.9 ± 0.3		2.76×10^4	2.60×10^3
20	51 ± 6.4	12.46 ± 0.57	8.31×10^6	1.24×10^6
30	**17 ± 2.1**		**$1.61 \times 10^{6\ b}$**	**$2.73 \times 10^{5\ b}$**
40	16.4 ± 2.4		4.01×10^5	4.74×10^4
50	8.6 ± 1.7		1.23×10^5	3.14×10^4
60	6.1 ± 0.7		2.68×10^4	3.43×10^3
70	5.9 ± 0.5		1.67×10^4	1.04×10^4
80	**4.9 ± 0.3**		**$1.02 \times 10^{4\ b}$**	**$1.60 \times 10^{3\ b}$**
20	51 ± 6.4	5.4 ± 0.33	4.10×10^5	8.89×10^4
30	**17 ± 2.1**		**$8.71 \times 10^{4\ b}$**	**$2.35 \times 10^{4\ b}$**
40	16.4 ± 2.4		2.79×10^4	6.84×10^3
50	8.6 ± 1.7		1.16×10^4	3.65×10^3
60	6.1 ± 0.7		5.93×10^3	1.02×10^3
70	5.9 ± 0.5		1.17×10^3	3.60×10^2
80	4.9 ± 0.3		3.77×10^2	9.58×10^1

[a] Relative humidity conditions and errors in the initial DEP content variable were not considered in the parameter estimation procedure. [b] Values in bold were not used in the parameter estimation procedure to serve as an independent validation set.

In order to model the effect of temperature and initial DEP content, values of temperature (in Kelvin), initial DEP content and $K_{CA\text{-}air,}$ as presented in Table 1, were used to adjust Eq. (6), as described in Sections 2.4 and 2.5, and estimated parameters are summarised in Table 2, along with their associated standard deviations. It is important to note that all estimated parameters were statistically significant within 95% confidence level according to the standard t-test (Box, G.P., Hunter, J.S., Hunter, 2005).

Table 2 – Parameter estimates and their associated standard deviations obtained from the fitting of Eq. (6) to the experimental values of $K_{CA\text{-}air}$. $F_{obj}(\theta)$ and Chi^2 limits for model adequacy are also summarised.

Coefficient	Estimate ± standard deviation
k_1	6.71 ± 0.26
k_2	0.520 ± 0.039

k_3	-0.011 ± 0.0012
k_4	-25.54 ± 3.98
k_5	-2.51 ± 0.64
k_6	0.088 ± 0.019
$F_{obj}(\theta)$	5.26
Chi^2 *limits for adequacy* [a]	3.247 < *Final SSE* < 20.48

[a] *Chi*^{2} limits are for 10 degrees of freedom and 95% confidence level.

Fig. 3 (a-c) illustrates predicted $K_{CA\text{-}air}$ (continuous lines) along with experimental values described previously, where an excellent agreement can be observed. The comparison between observed and predicted $K_{CA\text{-}air}$ is also illustrated in Fig. 4, where results obtained across the 21 investigated experimental conditions are illustrated in logarithmic scale as a function of the initial DEP content for easier visualization. As is can be seen, an excellent agreement can be observed at temperature conditions lower than 50 ˚C, with a good agreement at the remaining conditions.

Model adequacy was further confirmed by the comparison between the final objective function ($F_{obj}(\theta)$) and the limits of the *Chi*^{2}-distribution, also illustrated in Table 2. Finally, our proposed model was also able to accurately predict $K_{CA\text{-}air}$ experimental measurements not used in the parameter estimation procedure (highlighted in bold in Table 1 and illustrated as '★' symbols in Fig. 3-4), supporting the validity of the developed model to predict $K_{CA\text{-}air}$ within the range of investigated conditions.

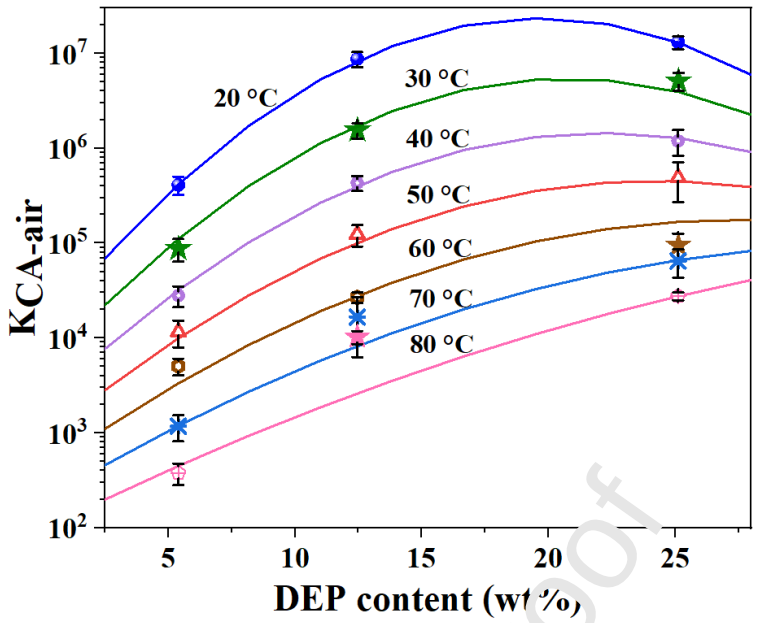

Fig. 4 - Experimental (scatter symbols) and predicted (continuous lines) values for $K_{CA\text{-}air}$ as a function of the initial DEP content for the different investigated temperatures. Symbols '★' in green, pink and brown colours indicate measurements used as independent validation set.

Finally, Table 3 summarises values for the DEP phase change enthalpy, ΔH°, for each sample composition, calculated using Eq. (8-9). As it can be seen, calculated enthalpies were slightly larger (in absolute terms) than the DEP condensation enthalpy at 298 K (-82.1 ± 1.6 kJ·mol^{-1} (Da Ros and Curran, 2021; Gobble et al., 2014; Roháč et al., 2004)), indicating that interactions between CA and DEP can be stronger than interactions within pure liquid DEP. This agrees with previous findings, where higher vaporisation enthalpies were reported for DEHP from vinyl floorings when compared to the vaporisation enthalpy of pure DEHP (Liang and Xu, 2014).

Table 3 – Resultant constants calculated using Eq. (8-9) with the estimated parameters as presented in Table 2 for each investigated composition, as detailed in Table 1.

Calculated constants	***6-DEP/CA***	***14-DEP/CA***	***22-DEP/CA***
ΔH° (kJ · mol^{-1}) [a]	-98.0	-115.9	-88.8

[a] ΔH° was calculated using Eq. (9), where the constant B was calculated using Eq. (8) with the estimated values of k_4, k_5 and k_6 (Table 2).

3.3 Simulated DEP loss

The ability of Eq. (6) to predict $K_{CA\text{-}air}$ is further illustrated by the comparison between experimental and simulated DEP losses calculated as described in Section 2.4, as illustrated in Fig. 5. Simulation error bars were calculated considering the variabilities introduced by the error in initial DEP contents, as detailed in Table 1. An excellent agreement between observed and simulated DEP loss values can be observed, further supporting the quality of the proposed $K_{CA\text{-}air}$ model.

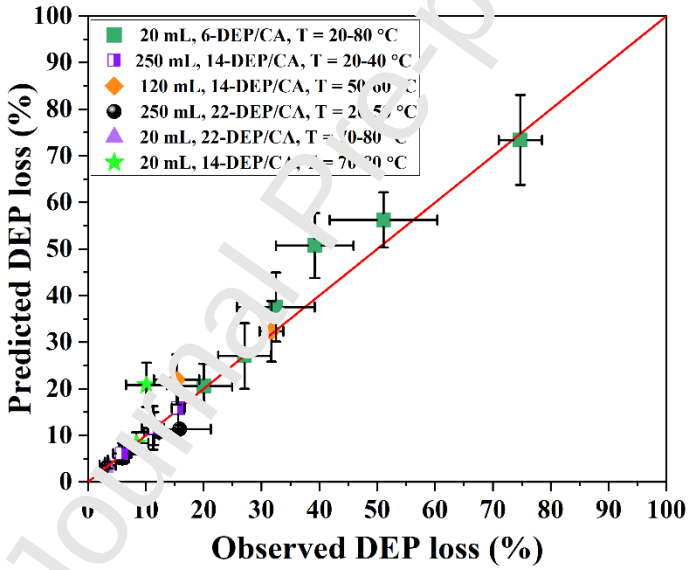

Fig. 5 – Comparison between observed experimental DEP losses and simulated values for *x-DEP/CA* samples equilibrated at different temperatures (partially illustrated in the figure) and sample enclosure vial volumes. Simulations were performed using the initial DEP content and temperature at each experimental condition, as summarised in Table 1.

3.4 Estimating $K_{CA\text{-}air}$ from DEP loss

In addition, the plasticiser migration model as described in Section 2.7 has been further employed to assess the validity of experimentally measured $K_{CA\text{-}air}$ values, by using it in combination with an additional group of experiments. In this case, *x-DEP/CA* samples were equilibrated for shorter periods of times at five selected experimental conditions (see *SI*), and the resulting quantified DEP losses as a function of time were used to fit the phenomenological model as described by Eqs. (12-16), where $K_{CA\text{-}air}$ and $D_{DEP\text{-}CA}$ were adjustable parameters estimated from the experimental data and Eq. (6) was not employed. Figs. S10-S14 in the *SI* illustrate experimental DEP loss values as a function of time for samples equilibrated at the different selected experimental conditions, where the DEP loss model is illustrated by the continuous blue line and estimated $K_{CA\text{-}air}$ and $D_{DEP\text{-}CA}$ values are summarised in Table S3 in the *SI*.

This analysis has demonstrated an excellent agreement between estimated and experimentally measured $K_{CA\text{-}air}$, as illustrated in Fig. S15, further supporting the consistency of experimental measurements used in the building of our $K_{CA\text{-}air}$ model (Eq. (6)).

3.5 Range of validity of Eq. (6).

It must be noted that experimental conditions investigated in this work involved sealed environments and temperatures ranging from 20 to 80 ˚C (as summarised in Table 1), where the relative humidity was allowed to vary according to temperature, resulting in relatively dry environments for temperatures equal or higher than 30 ˚C. Thus, while developed $K_{CA\text{-}air}$ model can be suitable for predicting DEP partitioning between CA and its surrounding environment within the explored experimental region, for instance, including 20 ˚C and 50% RH, we do not expect it to be valid for predicting $K_{CA\text{-}air}$ at experimental regions outside investigated ranges, for instance, including high temperatures and high and medium relative humidities. Further work is required to enable the expansion of the

experimental range where the model can be valid. Additionally, further work is also required to test the validity of our developed model to cellulose acetate materials presenting other shapes or thicknesses.

4. Discussion

The DEP partitioning from indoor built materials has been evaluated for a few systems (Da Ros and Curran, 2021), including cotton and rayon fabrics (Eftekhari and Morrison, 2018; Morrison et al., 2015; Saini et al., 2017), and latex paint (Schripp et al., 2014). For instance, Morrison *et al.* (Morrison et al., 2015) reported DEP partition coefficients between cotton fabric and air as equal to 2.5-7.7 $\times$ 10^5 at 25 ˚C. In another study, DEP partition coefficients between cotton fabric and air were demonstrated to vary exponentially with temperature (Eftekhari and Morrison, 2018), being reduced from 5.6 $\times$ 10^5 to 0.75 $\times$ 10^5 as the temperature was increased from 20 to 40 ˚C. DEP partition coefficients equal to 6.3 $\times$ 10^5 and 1.58 $\times$ 10^6 have also been reported for cotton and rayon fabrics equilibrated between 25-35 ˚C (Saini et al., 2017). For latex paint, higher DEP partition coefficients have been reported, with values ranging between 1.66 $\times$ 10^7 and 2.04 $\times$ 10^7 at approximately 23.5 ˚C, for two paint formulations initially containing 0.6 and 1wt% DEP, respectively, suggesting that DEP may have a larger tendency to absorb in latex paint than in cotton fabric (Schripp et al., 2014).

When compared to the above-mentioned studies, it is interesting to note that the $K_{CA\text{-}air}$ values determined in this work are of the same orders of magnitude, as illustrated in Table S4 in the *SI*, and that the $K_{CA\text{-}air}$ values obtained for *22-DEP/CA* samples are larger than the values obtained for cotton fabric, being more similar to values reported to the latex paint. As a greater hydrophilic character would be expected from cotton when compared to plasticised CA, a larger tendency for DEP to remain absorbed in the CA matrix was expected, explaining

and supporting larger $K_{CA\text{-}air}$ values. The hydrophobic nature of DEP in CA is further discussed in our previous work (del Gaudio et al., 2021).

In addition, even though studies quantifying phthalates partitioning in indoor building materials usually disregard concentration changes in the emitter phase, it is interesting to note the suggested effect of DEP composition on the partition coefficients reported for latex paint, as in this case, larger values were observed for the paint containing more DEP (Schripp et al., 2014). This agrees with our study, where $K_{CA\text{-}air}$ was demonstrated to vary in the same way with the initial DEP content. A similar effect of plasticiser concentration can also be inferred from results presented by Liang and Xu (Liang and Xu, 2014), who assessed the effect of temperature on phthalate emissions from vinyl flooring and mattress cover samples. In their study, the authors analysed, among other materials, vinyl floorings containing three different DEHP concentrations (0.1, 7 and 23wt%) and their results indicate an increase in the DEHP partition coefficient with the increase of the initial material-phase DEHP concentration, this behaviour being consistently observed at four different temperatures between 25 and 55 ˚C. In addition, these authors also noted the role played by the DEHP content on the relationship between DEHP partition coefficient and temperature, in agreement with our study.

Therefore, we hypothesise that changes in the nature of polymer-plasticiser interactions can occur as a function of the DEP composition in CA and that this effect can be related to the miscibility range between CA and DEP, which has been reported to be limited to DEP contents up to approximately 25wt% (Bao et al., 2015). Further research using DEP plasticised CA presenting contents higher than 25wt% would be useful for verifying our hypothesis. Additionally, it must be noted that determining if and how $K_{CA\text{-}air}$ varies continuously as the DEP content of a specific sample changes over time is beyond the scope of this paper.

To the best of our knowledge, this is the first work reporting DEP partition coefficients between CA and its surrounding atmosphere, where the effects of temperature and initial DEP content are simultaneously quantified and described by a mathematical model. Nevertheless, as discussed above, our results are in agreement with previous reports. Additionally, it is also worth noting the agreement between experimental $K_{CA\text{-}air}$ and values estimated using the phenomenological description of DEP migration applied to DEP loss data acquired at short equilibration times, as presented in in Section 3.4. In this case, estimated diffusion coefficients have also demonstrated a good agreement with previous findings on DEP diffusivity. For instance, Yuan *et al* (Yuan et al., 2019) reported DEP diffusion coefficients in polyvinyl chloride (PVC) as varying between $5.48 \cdot 10^{-17}$ and $3.99 \cdot 10^{-14}$ $m^2 \cdot s^{-1}$ for plasticised PVC films (containing 5 wt% DEP) in contact with different food simulants based on ethanol, *n*-hexane and isooctane at between 40 and 60 ˚C.

Furthermore, even though care has been taken to minimise the time between sample collection and analysis, it is possible that our results may present uncertainties arising from unavoidable DEP losses during analysis, which may have resulted in losses being overestimated to some extent, despite their consistent stability over time. This, in turn, may have affected experimentally determined $K_{CA\text{-}air}$, artificially reducing their values. However, we note that this effect, while likely present, would not invalidate obtained relationships for $K_{CA\text{-}air}$, as all experiments have been carried out using the same methodology. Additional sources of uncertainty could also arise from the different sample enclosure vials employed, which could present slightly different surface roughness (Wu et al., 2017) and therefore slightly different DEP glass and aluminum partition coefficients from the ones considered (Da Ros and Curran, 2021). Further work is required for enabling the determination of more precise DEP partition coefficients in CA.

Finally, it should be noted that further studies are also required to assess the impact of additional environmental conditions on the diethyl phthalate partitioning behaviour, for instance, including well-ventilated (and not sealed) scenarios. However, we note that sealed environments are commonly used as a method of storage in museum collections and archives, where minimising the extent to which an artefact perceives external fluctuations in temperature and relative humidity is a common aim. Thus, we believe that this work will have wide applications not only while describing real environments in the conservation field but also while assessing levels of human exposure in indoor environments where rates of air exchange and ventilation are low.

By quantitively describing the migration of DEP from CA-based materials, enabled in this work by our determination of $K_{CA\text{-}air}$ partition coefficients, we are contributing to increasing our understanding of how environmental conditions and sample properties can impact the overall rate of material decay, including physical damage promoted by plasticiser loss. The work also increases understanding of how consumer goods including DEP plasticised CA can contribute to increasing levels of this phthalate in indoor environments.

5. Conclusions

This work has investigated the partitioning behaviour of diethyl phthalate (DEP) between cellulose acetate (CA) and its surrounding air at a wide range of temperatures, and plasticiser concentrations, for the first time. Our results indicate that both investigated variables have a statistically significant impact on DEP partition coefficients, $K_{CA\text{-}air}$: while it is exponentially reduced as temperature rises, it increases non-linearly as a function of DEP content. At 20 ˚C, quantified $K_{CA\text{-}air}$ values ranged between $4.1 \cdot 10^6 \pm 8.9 \cdot 10^4$ and $1.3 \cdot 10^7 \pm 2.9 \cdot 10^6$ among sample compositions, in agreement with previous reports on DEP partitioning on cotton fabrics.

Additionally, we propose and validate a novel mathematical model to describe the relationship among $K_{CA\text{-}air}$, temperature and DEP content in CA, where parameters have been estimated using measurements from 130 distinct experiments and their statistical characterisation is fully evaluated. The suitability of our model to predict $K_{CA\text{-}air}$ has also been demonstrated by its application to simulate the DEP migration from CA-based materials.

We anticipate that both experimentally measured $K_{CA\text{-air}}$ and our developed $K_{CA\text{-air}}$ model will be of great value for enabling precise mathematical descriptions of degradation phenomena involving plasticiser loss in cellulose acetate-based museum artefacts, contributing to ongoing efforts dedicated to their preservation in cultural heritage collections. Additionally, we hope this work will also contribute to determining levels of human exposure to this and additional phthalates present in indoor built materials and consumer goods.

6. Acknowledgments

This project has received funding from the European Research Council (ERC) under the European Union's Horizon 2020 research and innovation programme (grant agreement No 716390). We thank UCL Chemistry and Turner Lab for access to ovens, and Dr. Luca Mazzei for interesting discussions.

7. References

Bao, C.Y., Long, D.R., Vergelati, C., 2015. Miscibility and dynamical properties of cellulose acetate / plasticizer systems. Carbohydr. Polym. 116, 95–102. https://doi.org/10.1016/j.carbpol.2014.07.078

Bickersteth, J., 2014. Environmental conditions for safeguarding collections: What should our set points be? Stud. Conserv. 59, 218–224. https://doi.org/10.1179/2047058414Y.0000000143

Box, G.P., Hunter, J.S., Hunter, W.G., 2005. Statistics for experimenters - Design,

innovation, and discovery, Second. ed. Wiley-Interscience, John Wiley & Sons, Inc., New Jersey. https://doi.org/10.1017/S1742170510000062

Cao, J., Weschler, C.J., Luo, J., Zhang, Y., 2016. Cm-History method, a novel approach to simultaneously measure source and sink parameters important for estimating indoor exposures to phthalates. Environ. Sci. Technol. 50, 825–834. https://doi.org/10.1021/acs.est.5b04404

Da Ros, S., Aliev, A.E., del Gaudio, I., King, R., Pokorska, A., Kearney, M., Curran, K., 2021a. Characterising plasticised cellulose acetate-based historic artefacts by NMR spectroscopy: A new approach for quantifying the degree of substitution and diethyl phthalate contents. Polym. Degrad. Stab. 183, 109420 https://doi.org/10.1016/j.polymdegradstab.2020.109420

Da Ros, S., Curran, K., 2021. Modelling and parameter estimation of diethyl phthalate partitioning behaviour on glass and aluminum surfaces. Chemosphere 131414. https://doi.org/10.1016/j.chemosphere.2021.131414

Da Ros, S., Curran, K., del Gaudio, I., Ormsby, B., Townsend, J.H., Cane, D., Gili, A., 2021b. Unveiling the importance of diffusion on the deterioration of cellulose acetate artefacts : The profile of plasticiser loss as assessed by infrared microscopy, in: Transcending Boundaries: Integrated Approaches to Conservation. ICOM-CC 19th Triennial Conference Preprints.

Da Ros, S., Schwaab, M., Pinto, J.C., 2017. Parameter estimation and Statistical Methods. Chem. Mol. Sci. Chem. Eng. 1–7. https://doi.org/10.1016/B978-0-12-409547-2.13918-6

del Gaudio, I., Hunter-Sellars, E., Parkin, I.P., Williams, D., Da Ros, S., Curran, K., 2021. Water sorption and diffusion in cellulose acetate: The effect of plasticisers. Carbohydr. Polym. 267, 118185. https://doi.org/10.1016/j.carbpol.2021.118185

Eftekhari, A., Morrison, G.C., 2018. A high throughput method for measuring cloth-air equilibrium distribution ratios for SVOCs present in indoor environments. Talanta 183, 250–257. https://doi.org/10.1016/j.talanta.2018.02.061

Fromme, H., Lahrz, T., Piloty, M., Gebhart, H., Oddoy, A., Ruden, H., 2004. Occurrence of phthalates and musk fragrances in indoor air and dust from apartments and kindergartens in Berlin (Germany). Indoor Air 14, 188–195. https://doi.org/10.1046/j.1600-0668.2003.00223.x

Gautam, V., Srivastava, A., Singh, K.P., Yadav, V.L., 2016. Vibrational and gravimetric analysis of polyaniline/polysaccharide composite materials. Polym. Sci. Ser. A 58, 206–219. https://doi.org/10.1134/s0965545x16020085

Gili, A.., King, R., Mazzei, L., Grau-Bové, J., Koestler, P., Petr, M., Maddene, O., Ros, S. Da, Curran, K., 2019. Modelling and measuring the diethyl phthalate plasticiser loss from cellulose acetate in different ventilation scenarios, in: The Plastics Heritage Congress 2019. History, Limits and Possibilities. Lisbon.

Gobble, C., Chickos, J., Verevkin, S.P., 2014. Vapor pressures and vaporization enthalpies of a series of dialkyl phthalates by correlation gas chromatography. J. Chem. Eng. Data 59, 1353–1365. https://doi.org/10.1021/je500110d

Huang, L., Jolliet, O., 2019. A quantitative structure-property relationship (QSPR) for estimating solid material-air partition coefficients of organic compounds. Indoor Air 29, 79–88. https://doi.org/10.1111/ina.12510

Huang, L., Jolliet, O., 2016. A parsimonious model for the release of volatile organic compounds (VOCs) encapsulated in products. Atmos. Environ. 127, 223–235. https://doi.org/10.1016/j.atmosenv.2015.12.001

Kennedy, J., Eberhart, R., 1995. Particle Swarm Optimization, in: Proceedings of the IEEE International Conference on Neural Networks. Perth, pp. 1942–1948.

https://doi.org/10.1109/ICNN.1995.488968

Koniecki, D., Wang, R., Moody, R.P., Zhu, J., 2011. Phthalates in cosmetic and personal care products: Concentrations and possible dermal exposure. Environ. Res. 111, 329–336. https://doi.org/10.1016/j.envres.2011.01.013

Liang, Y., Xu, Y., 2014. Emission of phthalates and phthalate alternatives from vinyl flooring and crib mattress covers: The influence of temperature. Environ. Sci. Technol. 48, 14228–14237. https://doi.org/10.1021/es504801x

Little, J.C., Hodgson, A.T., Gadgil, A.J., 1994. Modeling emissions of volatile organic compounds from new carpets. Atmos. Environ. 28, 227–234. https://doi.org/10.1016/1352-2310(94)90097-3

Liu, X., Guo, Z., Roache, N.F., 2014. Experimental method development for estimating solid-phase diffusion coefficients and material/air partition coefficients of SVOCs. Atmos. Environ. 89, 76–84. https://doi.org/10.1016/j.atmosenv.2014.02.021

Miles-Richardson, S.R., 2017. Public health implications of phthalates: a review of findings from the U.S. national toxicology program's expert panel reports, in: Wypych, G. (Ed.), Handbook of Plasticizers. ChemTec Publising, pp. 708–720.

Mondal, S., Mukherjee, S., 2020. Long-term dietary administration of diethyl phthalate triggers loss of insulin sensitivity in two key insulin target tissues of mice. Hum. Exp. Toxicol. 39, 984–993. https://doi.org/10.1177/0960327120909526

Morrison, G., Li, H., Mishra, S., Buechlein, M., 2015. Airborne phthalate partitioning to cotton clothing. Atmos. Environ. 115, 149–152. https://doi.org/10.1016/j.atmosenv.2015.05.051

Noronha, F.B., Pinto, J.C., Monteiro, J.L., Lobao, M.W., Santos, T.J., 1993. ESTIMA: Um pacote computacional para estimação de parâmetros e Pprojeto de experimentos. Rio de Janeiro.

Petzold, L.R., 1982. A description of DASSL: A Differential/Algebraic system solver, in: IMACA World Congress. Montreal, pp. 1–11. https://doi.org/https://www.osti.gov/servlets/purl/5882821

Pinto, J.C., Lage, P.L.C., 2001. Métodos numéricos em problemas de Engenharia Química, 01st ed. e-papers, Rio de Janeiro.

Puls, J., Wilson, S.A., Hölter, D., 2011. Degradation of Cellulose Acetate-Based Materials: A Review. J. Polym. Environ. https://doi.org/10.1007/s10924-010-0258-0

Rajeswari, A., Christy, E.J.S., Swathi, E., Pius, A., 2020. Fabrication of improved cellulose acetate-based biodegradable films for food packaging applications. Environ. Chem. Ecotoxicol. 2, 107–114. https://doi.org/10.1016/j.enceco.2020.07.003

Richardson, E., Truffa Giachet, M., Schilling, M., Learner, T., 2014. Assessing the physical stability of archival cellulose acetate films by monitoring plasticizer loss. Polym. Degrad. Stab. 107, 231–236. https://doi.org/10.1016/j.polymdegradstab.2013.12.001

Roháč, V., Růžička, K., Růžička, V., Zaitsau, D.H., Kabo, G.J., Diky, V., Aim, K., 2004. Vapour pressure of diethyl phthalate. J. Chem. Thermodyn. 36, 929–937. https://doi.org/10.1016/j.jct.2004.07.025

Saini, A., Okeme, J.O., Mark Parnis, J., McQueen, R.H., Diamond, M.L., 2017. From air to clothing: characterizing the accumulation of semi-volatile organic compounds to fabrics in indoor environments. Indoor Air 27, 631–641. https://doi.org/10.1111/ina.12328

Schripp, T., Salthammer, T., Fauck, C., Bekö, G., Weschler, C.J., 2014. Latex paint as a delivery vehicle for diethylphthalate and di-n-butylphthalate: Predictable boundary layer concentrations and emission rates. Sci. Total Environ. 494–495, 299–305. https://doi.org/10.1016/j.scitotenv.2014.06.141

Schwaab, M., Biscaia, E.C., Monteiro, J.L., Pinto, J.C., 2008. Nonlinear parameter estimation through particle swarm optimization. Chem. Eng. Sci. 63, 1542–1552.

https://doi.org/10.1016/j.ces.2007.11.024

Schwaab, M., Pinto, J.C., 2007. Analise de Dados Experimentais I - Fundamentos de Estatística e Estimação de Parâmetros. e-papers, Rio de Janeiro.

Sheu, R., Fortenberry, C.F., Walker, M.J., Eftekhari, A., Stönner, C., Bakker, A., Peccia, J., Williams, J., Morrison, G.C., Williams, B.J., Gentner, D.R., 2021. Evaluating Indoor Air Chemical Diversity, Indoor-to-Outdoor Emissions, and Surface Reservoirs Using High-Resolution Mass Spectrometry. Environ. Sci. Technol. 55, 10255–10267. https://doi.org/10.1021/acs.est.1c01337

Sutherland, K., Schwarzinger, C., Price, B.A., 2012. The application of pyrolysis gas chromatography mass spectrometry for the identification of degraded early plastics in a sculpture by Naum Gabo. J. Anal. Appl. Pyrolysis 94, 202–208. https://doi.org/10.1016/j.jaap.2011.12.016

Wei, W., Mandin, C., Ramalho, O., 2018. Influence of indoor environmental factors on mass transfer parameters and concentrations of semi-volatile organic compounds. Chemosphere 195, 223–235. https://doi.org/10.1016/j.chemosphere.2017.12.072

Wu, Y., Eichler, C.M.A., Leng, W., Cox, S.S., Marr, L.C., Little, J.C., 2017. Adsorption of Phthalates on Impervious Indoor Surfaces. Environ. Sci. Technol. 51, 2907–2913. https://doi.org/10.1021/acs.est.6b05853

Xu, Y., Little, J.C., 2006. Predicting emissions of SVOCs from polymeric materials and their interaction with airborne particles. Environ. Sci. Technol. 40, 456–461. https://doi.org/10.1021/es051517j

Yang, C., Harris, S.A., Jantunen, L.M., Kvasnicka, J., Nguyen, L. V., Diamond, M.L., 2020. Phthalates: Relationships between air, dust, electronic devices, and hands with implications for exposure. Environ. Sci. Technol. 54, 8186–8197. https://doi.org/10.1021/acs.est.0c00229

Yuan, H., Hao, Q., Su, R., Qi, W., He, Z., 2019. Migration of phthalates from polyvinyl chloride film to fatty food simulants: experimental studies and model application. J. fur Verbraucherschutz und Leb. 15, 135–143. https://doi.org/10.1007/s00003-019-01249-x

Credit author statement

Simoní Da Ros: Conceptualisation; Methodology; Investigation; Formal Analysis; Visualisation; Writing – Original Draft; Writing – Review & Editing.

Argyro Gili: Methodology; Writing – Review & Editing.

Katherine Curran: Conceptualisation, Writing – Review & Editing; Project administration; Funding Acquisition.

Declaration of interests

☒ The authors declare that they have no known competing financial interests or personal relationships that could have appeared to influence the work reported in this paper.

☐The authors declare the following financial interests/personal relationships which may be considered as potential competing interests:

Graphical abstract

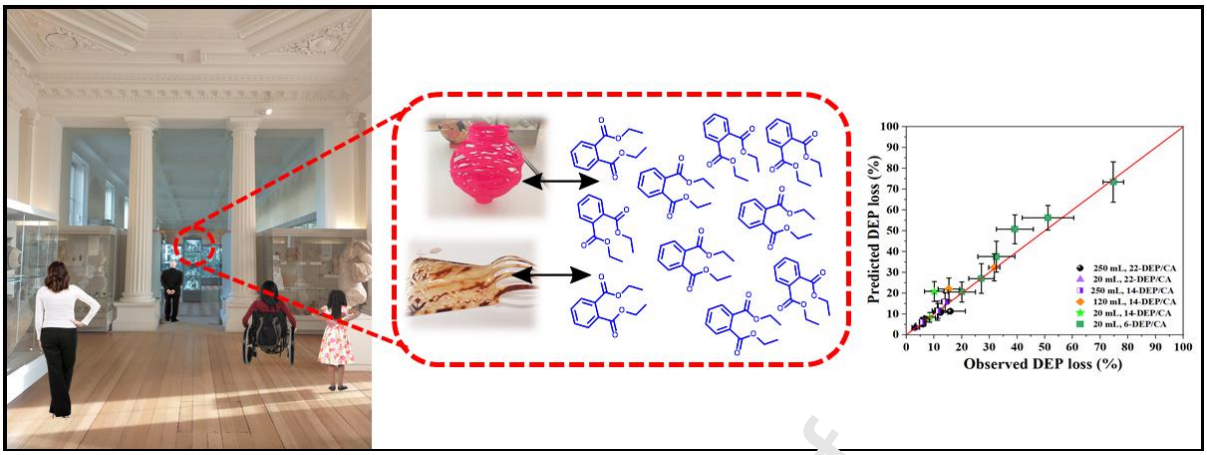

Highlights

- We assess diethyl phthalate (DEP) partitioning in cellulose acetate (CA).
- Temperature and plasticiser composition effects are quantified.
- A mathematical relationship for predicting DEP partitioning is presented.
- Implications for describing the migration of this compound from CA are discussed.